Cell type-specific network analysis in Diversity Outbred mice identifies genes potentially responsible for human bone mineral density GWAS associations

Luke J Dillard[1], Gina M Calabrese[1], Larry D Mesner[1,2], Charles R Farber[1,2,3]

[1]Center for Public Health Genomics, School of Medicine, University of Virginia, Charlottesville, VA 22908
[2]Department of Public Health Sciences, School of Medicine, University of Virginia, Charlottesville, VA 22908
[3]Department of Biochemistry and Molecular Genetics, School of Medicine, University of Virginia, Charlottesville, VA 22908

Correspondence to:

Charles R. Farber
E-mail: crf2s@virginia.edu
Center for Public Health Genomics
University of Virginia
P.O. Box 800717
Charlottesville, VA 22908, USA

Tel. 434-243-8584

Summary

Genome-wide association studies (GWASs) have identified many sources of genetic variation associated with bone mineral density (BMD), a clinical predictor of fracture risk and osteoporosis. Aside from the identification of causal genes, other difficult challenges to informing GWAS include characterizing the roles of predicted causal genes in disease and providing additional functional context, such as the cell type predictions or biological pathways in which causal genes operate. Leveraging single-cell transcriptomics (scRNA-seq) can assist in informing BMD GWAS by linking disease-associated variants to genes and providing a cell type context for which these causal genes drive disease. Here, we use large-scale scRNA-seq data from bone marrow–derived stromal cells cultured under osteogenic conditions (BMSC-OBs) from Diversity Outbred (DO) mice to generate cell type-specific networks and contextualize BMD GWAS-implicated genes. Using trajectories inferred from the scRNA-seq data that map cell state transitions, we identify networks enriched with genes that exhibit the most dynamic changes in expression across trajectories. We discover 21 network driver genes, which are likely to be causal for human BMD GWAS associations that colocalize with expression/splicing quantitative trait loci (eQTL/sQTL). These driver genes, including *Fgfrl1* and *Tpx2*, along with their associated networks, are predicted to be novel regulators of BMD via their roles in the differentiation of mesenchymal lineage cells. In this work, we showcase the use of single-cell transcriptomics from mouse bone-relevant cells to inform human BMD GWAS and prioritize genetic targets with potential causal roles in the development of osteoporosis.

Keywords: Osteoblasts, Osteocytes, Osteoporosis, Mesenchymal Stem Cells (MSC), Stromal cells, Systems Biology

Introduction

Osteoporosis is a complex disease characterized by low bone mineral density (BMD), bone fragility, and an increased risk of fracture[1]. BMD, a highly heritable trait, is one of the most important clinical predictors of osteoporotic fracture[2,3]. Increasing our understanding of the genetic basis of BMD is critical for the development of approaches for the treatment and prevention of osteoporosis. In recent years, genome-wide association studies (GWAS) have made great progress in unraveling BMD genetics by identifying over 1,100 independent associations[4]. Now the challenge lies in pinpointing causal genes, which is necessary for the translation of genetic findings into novel therapies.

A number of approaches exist to identify genes responsible for GWAS associations[5–8]. Most rely on population-based “-omics” data[9], which are scarce for human bone, to connect associations to causal genes. Our group has used co-expression networks generated from mouse bone transcriptomic datasets to assist in the identification of genes likely responsible for BMD associations. One significant advantage of this approach is its ability to utilize the network connections of candidate genes to predict how these candidate genes may affect BMD. For example, we generated co-expression networks from bone tissue and primary osteoblasts in mouse genetic reference populations and identified multiple co-expression modules enriched with genes located in BMD associations[10,11]. We then cross-referenced genes in these modules with those regulated by co-localizing expression quantitative trait loci (eQTLs) from the Gene-Tissue Expression project (GTEx)[12,13] to identify "high priority" genes. Recently, we expanded our analyses to include directed networks generated via a Bayesian approach using cortical bone RNA-seq data from 192 Diversity Outbred (DO) mice. By combining key driver analysis and

GTEx eQTL colocalization data, we identified 19 novel genes, such as *SERTAD4* and *GLT8D2*, which are likely causal for human BMD GWAS associations[14].

To date, our analyses have been reliant on networks generated from heterogeneous bulk transcriptomics (RNA-seq) datasets from mouse bone and primary bone cells. However, leveraging single-cell transcriptomics (scRNA-seq) data would offer the added benefit of resolving the transcriptomic profiles of discrete cell types. Additionally, using scRNA-seq data has the potential to provide context by predicting the specific cell types in which causal genes and their associated networks operate. In recent work, we demonstrated the utility of bone marrow-derived stromal cells cultured under osteogenic condition (BMSC-OB) for the generation of population-scale scRNA-seq data on bone relevant cell types[15]. The BMSC-OB model effectively enriches for mesenchymal lineage cells (e.g., mesenchymal progenitors, osteoblasts, osteocyte-like cells) that are highly relevant to the regulation of BMD.

In this work, our goal was to prioritize and contextualize genes implicated by BMD GWAS using an expanded large-scale (N=80) BMSC-OB scRNA-seq dataset on bone cell types. We accomplished this by first generating co-expression and Bayesian networks[14] for each BMSC-OB mesenchymal cell type. We subsequently prioritized networks based on their enrichment for genes exhibiting the most dynamic changes in expression across trajectories inferred from the scRNA-seq data, thus highlighting networks likely associated with the differentiation of BMSC-OBs. We then used these networks linked to osteogenic differentiation to prioritize genes with eQTL and/or splicing quantitative trait loci (sQTL) which colocalize with BMD GWAS associations[7,16]. In doing so, this analysis provides additional support for a role of these genes in the regulation of BMD and highlights their potential roles in differentiation of cell types essential to skeletal health.

Results

BMSC-OBs derived from DO mice yield diverse cell types that are enriched for mesenchymal lineage cells:

We cultured BMSCs from a total of 80 Diversity Outbred (DO) mice, a genetically diverse outbred mouse population[17,18] (N=75 from the current study and N=5 from[15]; N□=□49 male and N□=□31 females). We cultured BMSCs under osteogenic conditions and subsequently performed scRNA-seq, as described in[15]. After stringent processing and quality control (Materials and Methods), the dataset consisted of 21,831 expressed genes across 139,392 cells. We manually annotated 15 clusters ranging in size from 270 to 27,291 cells and identified cell types of the mesenchymal lineage as well as various other cell types (**Fig. 1A**, **Supplementary Table S1**).

Based on our prior BMSC-OB scRNA-seq study[15], we expected to identify a large proportion of mesenchymal cells and a smaller fraction of non-mesenchymal cell types. Consistent with this hypothesis, clusters associated with mesenchymal lineages accounted for 74.1% of all cells (**Fig. 1A**). These included mesenchymal progenitor cells (MPCs), late mesenchymal progenitors (LMPs), osteoblast progenitors (OBPs), two mature osteoblast populations (OB1 and OB2), osteocyte-like cells (Ocy), and marrow adipogenic lineage progenitors (MALPs). The non-mesenchymal cell types observed included macrophages, monocytes, granulocytes, T-cells, B-cells, endothelial cells, and osteoclast-like cells (**Fig. 1A**). With regards to the mesenchymal cell types, the only differences in cell clusters relative to our previous report[15] were the presence of MPCs and two mature osteoblast clusters. Upon comparing the two distinct osteoblast clusters, OB1 and OB2 (**Fig. 1A**), both clusters had ubiquitous expression of genes associated with mature osteoblasts (e.g., *Col1a1*, *Bglap*, *Sparc*,

and *Ibsp*) (**Supplementary Table S1**) while many of the "canonical" osteoblast markers were more highly expressed in OB1 compared to OB2 (**Supplementary Table S2**). Interestingly, MPCs did not have transcriptomic profiles similar to other mesenchymal progenitor cells previously identified by our group or others[15,19]. All other mesenchymal cell types demonstrated specific expression of canonical marker genes (**Fig. 1A, B**).

We next assessed the variability in cell type frequencies across DO mice by quantifying the proportions of each annotated mesenchymal cell type. All other clusters, which mainly consisted of immune cells of hematopoietic origin, were aggregated into one group (Hem) for each mouse. We observed high variability in the raw proportional abundances of cell types derived from each mouse (**Fig. 1C, Supplementary Table S3**). For example, the proportions of osteoblasts (OB1 and OB2) varied significantly among individual DO mice (**Fig. 1D**). All mice used in the current experiment had been extensively phenotyped for a wide range of bone traits (microCT, histomorphometry, biomechanical bone properties, etc.) as part of a previous genetic analysis of bone strength[14]. We correlated cell type frequencies with bone traits, however, none of the cell type proportions were strongly correlated with any bone trait (**Supplementary Table S4, S5**).

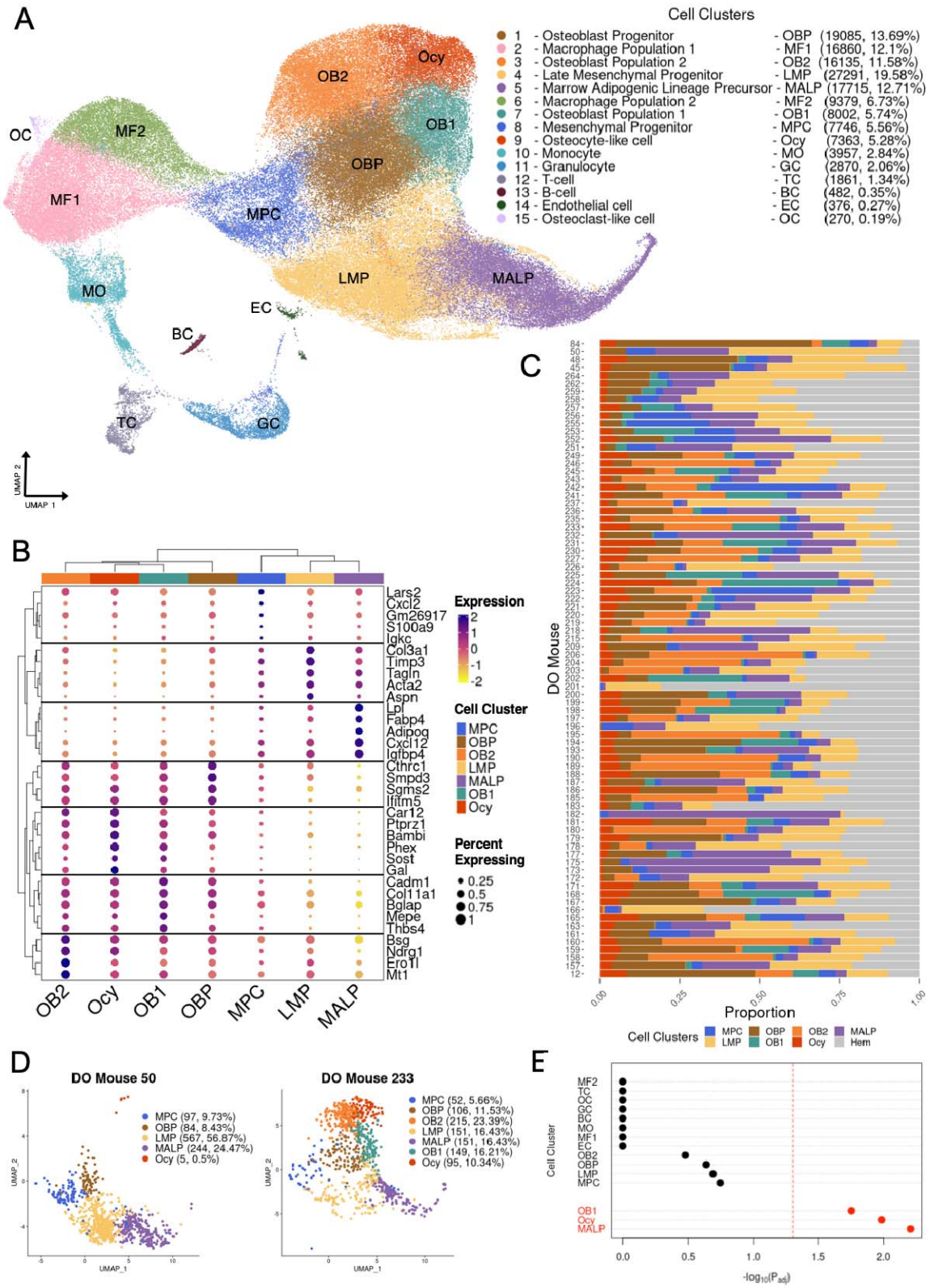

Figure 1. Analysis of single cell RNA-seq (scRNA-seq) data for BMSC-OBs derived from 80 Diversity Outbred (DO) mice.

Mesenchymal lineage cells are enriched in BMD heritability:

The primary goal of this work was to prioritize and contextualize genes implicated by BMD GWAS. As a first step towards this goal, we sought to determine which cell types were the most relevant to the genetics of BMD. Using the BMD GWAS and the BMSC-OB scRNA-seq data, we performed a CELLECT[20] cell type prioritization analysis to identify cell clusters enriched for BMD heritability. We observed that OB1, Ocy, and MALP cell clusters were significantly enriched ($P_{adj} < 0.05$, red dashed line) for BMD heritability ($P_{adj} = 0.018$, 0.010, 0.006, respectively) (**Fig. 1E**, **Supplementary Tables S6**). None of the non-mesenchymal cells identified were significant ($P_{adj} > 0.05$) (**Fig. 1E**). As a result, all downstream efforts focused solely on using data on mesenchymal cell types to inform GWAS.

Generating mesenchymal cell type-specific Bayesian networks to inform BMD GWAS:

We have previously shown that network-based approaches using bulk RNA-seq are powerful tools for the identification of putative causal genes from BMD GWAS data[10,11,14]. Here, our goal was to apply these same approaches using the BMSC-OB scRNA-seq data to prioritize and contextualize genes we previously identified as having a colocalizing expression quantitative trait locus (eQTL; N=512) or splicing QTL (sQTL; N=732) in a tissue from the Genotype-Tissue Expression (GTEx) project[7,13,16]. Genes identified in each study (or both) yielded a list of high priority target genes (N = 1,037). While GTEx does not currently contain data for bone tissue, eQTL can be shared across many tissues and may exert their effects in cell types resident to bone[21]. Therefore, utilizing our previous work, we hypothesized that generating cell type-specific networks would yield more biologically relevant representations of processes occurring within particular mesenchymal cell types. Additionally, by integrating GWAS, cell type-specific

networks, and dynamic gene expression as a function of differentiation, we anticipated we would identify points of intervention in which genetic variation impacts genes involved in the differentiation process.

Our network analysis begins by partitioning genes into groups based on co-expression by applying iterative weighted gene co-expression network analysis (iterativeWGCNA)[22] to each mesenchymal cell type (Step 1, **Fig. 2**). In total, 535 modules were identified from the BMSC-OB scRNA-seq data, and the number of modules identified for each mesenchymal cell cluster ranged from 26 to 153 with an average of 76 modules per cluster (**Supplementary Table S7, S8**). We sought to infer causal relationships between genes in each cell type-specific co-expression module and subsequently identify networks involved in processes relevant to BMSC-OB differentiation. To this end, we generated Bayesian networks for each co-expression module, thus enabling us to model directed interactions between co-expressed genes based on conditional independence[14] (Step 2, **Fig. 2**).

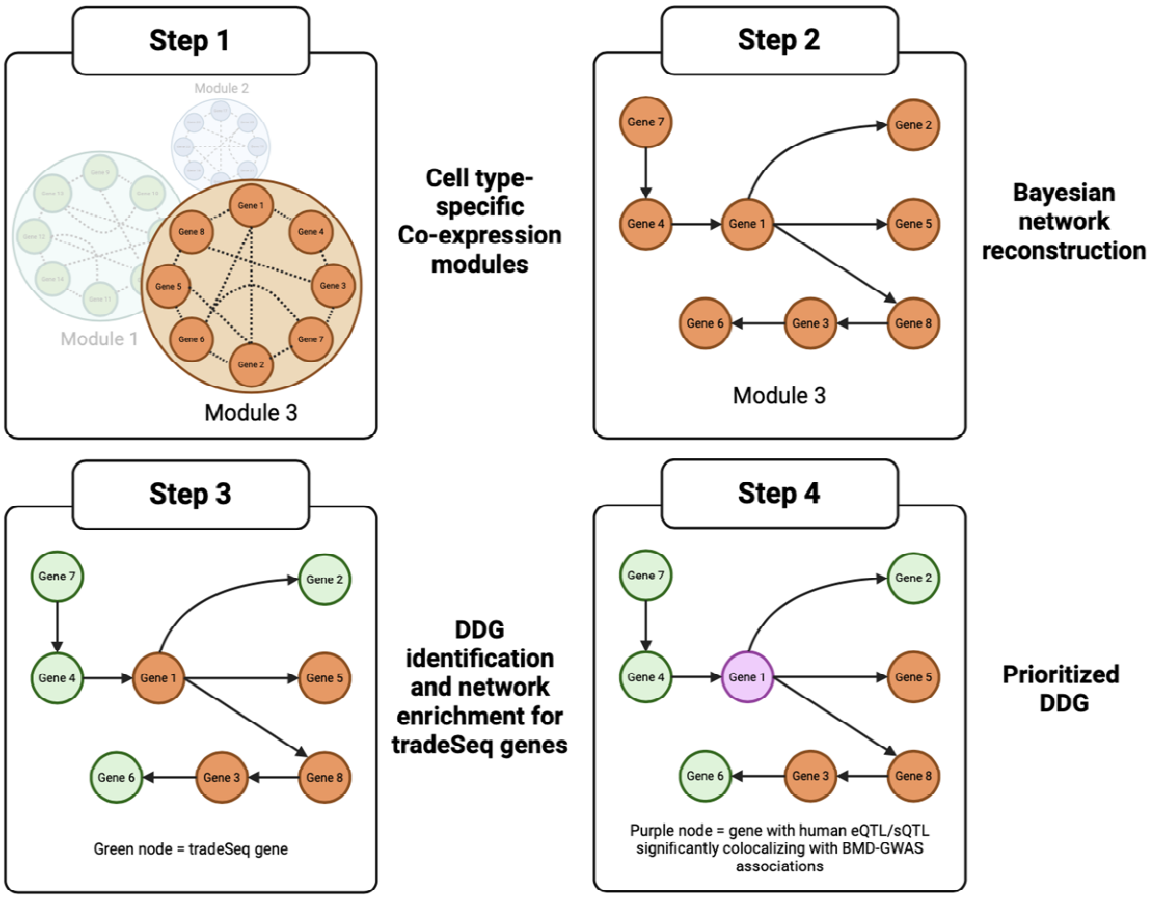

Figure 2. Overview of the network analysis pipeline

Identifying putative drivers of mesenchymal cell differentiation:

We hypothesized that many genes impacting BMD do so by influencing osteogenic differentiation or possibly bone marrow adipogenic differentiation of key mesenchymal cell types, as suggested by the CELLECT analysis above. Therefore, the next step of our network analysis was to identify cell type-specific Bayesian networks enriched for genes potentially driving mesenchymal differentiation (Step 3, **Fig. 2**). To accomplish this, we first performed a pseudotime trajectory analysis to infer paths of differentiation in the mesenchymal lineage cells. We resolved three pseudotime trajectories (two osteogenic, one adipogenic) originating from the

MPC cell cluster and ending in either Ocy, OB2, or MALP cell fates (**Fig. 3A**). It is important to note that given the identification of multiple skeletal stem cells[23–26], we do not view these trajectories as lineages, but rather "differentiation paths" (progenitor to mature and/or terminally differentiated cells) that are likely traversed by different subsets of skeletal stem cells.

To identify genes likely impacting BMSC-OB differentiation, we used tradeSeq to identify genes that exhibit dynamic changes in expression along pseudotime[27]. Prior to performing the tradeSeq analysis, we parsed the pseudotime trajectories into regions that encompass cells associated with each cell type along their respective trajectories (**Fig. 3B**). We defined multiple cell type boundaries (nine in total) using pseudotime values, which represent points along a trajectory. The tradeSeq analysis was performed for each boundary (**Supplementary Table S9**). For example, trajectories bifurcate in the LMP cell cluster (**Fig. 3A**); therefore, cells belonging to the LMP cluster can map to adipogenic and/or osteogenic trajectories depending on their placement along pseudotime. Between a cell type boundary, cells spanning a specific cluster (e.g., LMP) and mapping to a specific trajectory (e.g., osteogenic trajectory) are used as input to analyze gene expression between the start and end points of the cell type boundary (e.g., LMP_to_OBP). We analyzed gene expression within the established cell type boundaries for all trajectories and identified genes that exhibit the most significant differences in expression between the start and end points of the cell type boundaries. The total number of significant trajectory-specific tradeSeq genes ($P_{adj} < 0.05$) ranged from 87 to 1,697 across the 9 cell type boundaries (**Supplementary Table S9, S10-12**). The expression of representative marker genes for all cell types as a function of pseudotime were consistent with boundaries defined for each cell type (**Fig. 3C**).

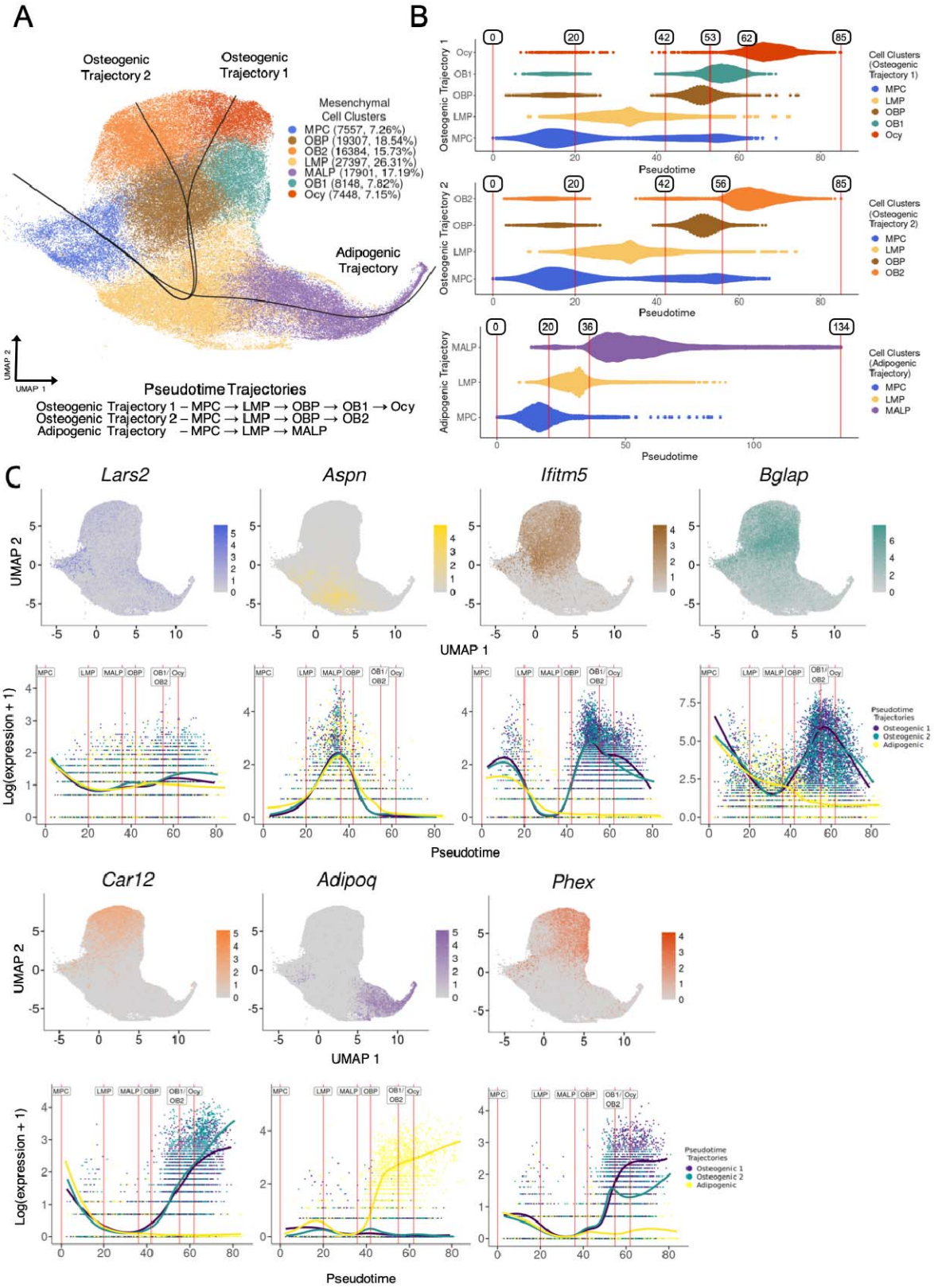

Figure 3. Pseudotime Trajectory Inference analysis and establishment of cell type boundaries for tradeSeq analysis

We sought to identify tradeSeq genes that may have associated expression quantitative trait locus (eQTL) and hypothesized that eQTLs that perturb their expression would also impact the proportion of cells at different stages along the cell trajectories. We performed a cell type-specific eQTL analysis for each mesenchymal cell type from the 80 DO mice scRNA-seq data. We identified 563 genes (eGenes) regulated by a significant *cis*-eQTL in specific cell types of the BMSC-OB scRNA-seq data (**Supplementary Table S14**). Despite being significantly underpowered for this analysis due to our relatively smaller sample size (N = 80), we identified two cell type-specific eGenes where the genotype responsible for the *cis*-eQTL effect was also associated with cell type proportions. The first of these genes was Pyruvate Kinase, muscle (*Pkm*), which was identified as a significant global tradeSeq gene (P_{adj} = 8.35 x 10^{-8}; **Supplementary Table S13**) associated with the transition from LMPs to OBPs along an osteogenic trajectory (**Fig. 4A**). Moreover, *Pkm* served as an eGene in the LMP cell cluster (LOD = 9.72; **Fig. 4B, Supplementary Table S14**). Mice inheriting at least one PWK allele at this locus (N = 15) demonstrated lower *Pkm* expression (**Fig. 4C**) and a notable reduction in mature osteoblasts (OB1) and osteocyte-like cells (Ocy) proportions (P = 0.030 and P = 0.026, respectively), while LMP proportions were unaffected (**Fig. 4D, Supplementary Table 15**).

Similarly, S100 calcium binding protein A1 (*S100a1*) was an OBP to OB1 transition tradeSeq gene (P_{adj} = 0.023; **Fig. 4A, Supplementary Table S13**) and an eGene in the OBP cell cluster (LOD = 10.12; **Fig. 4B, Supplementary Table S14**). Mice inheriting at least one 129 allele at this locus (N = 30) had higher *S100a1* expression, while the opposite was observed for mice inheriting NZO alleles (N = 14) (**Fig. 4C**). Additionally, mice inheriting at least one 129 allele showed a significant decrease in LMP proportion and increase in OB1 proportion (P = 0.008 and P = 0.016, respectively) (**Fig. 4D, Supplementary Table S15**), while no significant

differences were observed in cell type proportions among mice inheriting NZO alleles at this locus (**Supplementary Fig. 2, Supplementary Table S15**).

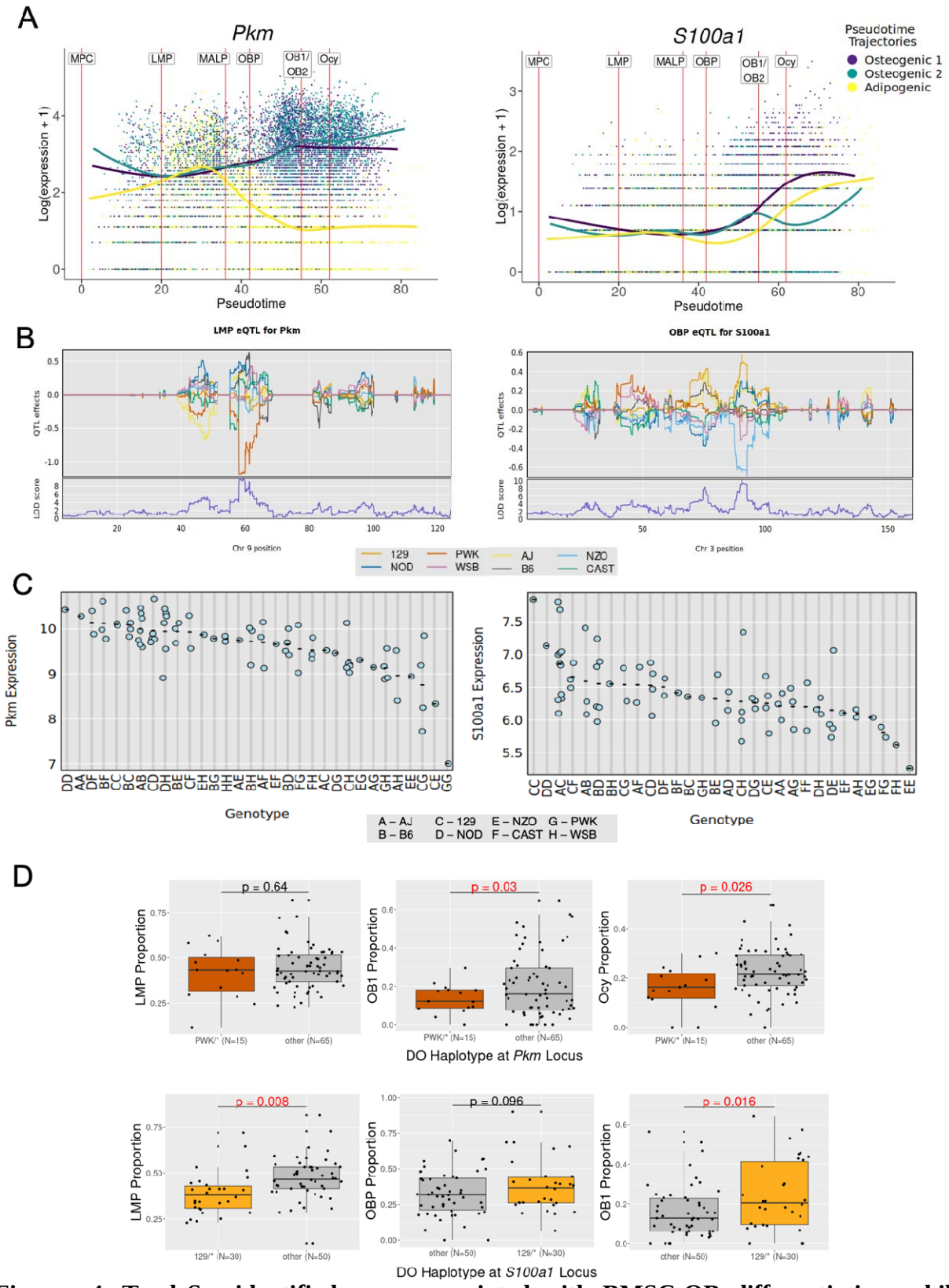

Figure 4. TradeSeq-identified genes associated with BMSC-OB differentiation exhibit eQTL effects.

Identification of differentiation driver genes (DDG):

In order to discover BMSC-OB differentiation genes potentially responsible for BMD GWAS associations, the next step of our network analysis leveraged the trajectory-specific tradeSeq genes identified for each cell type boundary (**Supplementary Table S10-12**) to identify differentiation driver genes (DDGs) (Step 3, **Fig. 2**). We identified DDGs by extracting subnetworks (i.e., large 3-step neighborhoods; see Methods) for each gene in each cell type-specific Bayesian network and identifying those subnetworks enriched ($P_{adj} < 0.05$) for trajectory-specific tradeSeq genes for the cell type boundary. The analysis identified 408 significant DDGs (**Supplementary Table S16, S17-19**). We performed a PANTHER[28] Gene Ontology (GO) analysis for the cell type boundaries yielding a sufficient number of DDGs and found that DDGs for the osteogenic cell type boundaries (LMP_to_OBP, OBP_to_OB1, OBP_to_OB2) were enriched for genes associated with the cell cycle (GO:0007049; N = 23, 18, 23; P = 1.12×10^{-6}, 1.29×10^{-13}, 1.0×10^{-14}, respectively) (**Supplementary Table S20-22**). The DDGs for the adipogenic cell type boundary (LMP_to_MALP, MALP_to_end) were enriched for genes associated with extracellular matrix organization (GO:0030198; N = 10; P = 1.62×10^{-7}) and lipid metabolic processes (GO:0006629; N = 25; P = 1.83×10^{-11}), respectively (**Supplementary Table S23-24**). Across all 408 DDGs, 49 (12%) were identified in one or more cell type boundaries as genes with a significant alteration (P < 0.05) of whole-body BMD when knocked-out/down in mice, as reported by the International Mouse Knockout Consortium (IMPC)[29] (**Supplementary Table S17-19**).

We used our previously generated list of potentially causal BMD GWAS genes (N=1,037) to subsequently prioritize the DDGs (Step 4, **Fig. 2**). Of the 408 DDGs, 21 DDGs in one or more cell type boundaries were genes that have BMD GWAS associations that colocalize

with sQTL/eQTL (**Table 1**). The majority of these DDGs were identified in LMPs along both the osteogenic (LMP_to_OBP) and adipogenic (LMP_to_MALP) trajectories (N = 10 and 6, respectively; **Supplementary Table S16, S25**). The remaining DDGs were identified in OBPs along both osteoblast trajectories (OBP_to_OB1, OBP_to_OB2; N = 1 and 3, respectively) and MALPs (MALP_to_end; N = 6). Additionally, 3 of the 21 DDGs (*Tet1*, *Tpx2*, *Timp2*) are IMPC genes that exhibit a significant alteration of BMD (**Supplementary Table S16, S25**).

Table 1: Prioritized Differentiation Driver Genes (DDGs) that have BMD GWAS associations that colocalize with splicing/expression QTL (eQTL/sQTL) identified in a Genotype-Tissue Expression project (GTEx) tissue. The tissue with the most significant colocalization (RCP and/or H4PP) is listed for each DGG (26 total, 21 distinct), as determined from Al-Barghouthi *et al.* (2022) and Abood *et al.* (2023) for eQTL and sQTL, respectively[7,16]. RCP = Regional Colocalization Probability (GWAS and eQTL colocalization). H4PP = H4 Posterior Probability (GWAS and sQTL colocalization).

Trajectory	**Cell type boundary**	**DDG**	**GTEx Tissue with strongest eQTL colocalization** (RCP)	**GTEx Tissue with strongest sQTL colocalization** (H4PP)	**eGene identified from scRNA-seq of the 80 DO mice**
1	LMP to OBP	*Tet1*	Adipose (Visceral); 0.3191	-	-
1	LMP to OBP	*Tpx2*	Testis; 0.2031	-	-
1	LMP to OBP	*Cdk1*	-	Pituitary; 0.7795	-
1	LMP to OBP	*Ttyh3*	-	Liver; 0.9350	-
1	LMP to OBP	*Olfml3*	Artery (Aorta); 0.8048	-	-
1	LMP to OBP	*Izumo4*	-	Brain (Hypothalamus); 0.9182	-
1	LMP to OBP	*Sec24d*	Nerve (Tibial); 0.2677		-
1	LMP to OBP	*Tmem263*	Adipose (Subcutaneous); 0.5704	Cultured cells (fibroblasts); 0.9716	-
1	LMP to OBP	*Lmf2*	-	Adrenal Gland; 0.8181	-
1	LMP to OBP	*Tln2*	Esophagus (Muscularis); 0.9697	-	-
1	OBP to OB1	*Kremen1*	Heart (Left Ventricle); 0.8686	-	-
2	OBP to OB2	*Kremen1*	Heart (Left Ventricle);	-	-

			0.8686		
2	OBP to OB2	*Ebf1*	-	Testis; 0.8760	-
2	OBP to OB2	*Lrp4*	Pancreas; 0.7943	-	-
3	LMP to MALP	*Ttyh3*	-	Liver; 0.9350	-
3	LMP to MALP	*Fgfrl1*	Cultured cells (fibroblasts); 0.1611	-	-
3	LMP to MALP	*Ebf1*	-	Testis; 0.8760	-
3	LMP to MALP	*Ppp1r12b*	-	Nerve (Tibial); 0.8807	-
3	LMP to MALP	*Rhoj*	Cultured cells (fibroblasts); 0.352	Breast; 0.7844	-
3	LMP to MALP	*Tln2*	Esophagus (Muscularis); 0.9697	-	-
3	MALP to end	*Adh1*	-	Esophagus (Gastroesophageal Junction); 0.9999	-
3	MALP to end	*Fgfrl1*	Cultured cells (fibroblasts); 0.1611	-	-
3	MALP to end	*Adcy5*	-	Esophagus (Gastroesophageal Junction); 0.8456	-
3	MALP to end	*Cnn2*	-	Spleen; 0.7743	-
3	MALP to end	*Mxra8*	-	Pituitary; 0.7545	-
3	MALP to end	*Timp2*	-	Testis; 0.9429	-

Network analysis predict *Fgfrl1* and *Tpx2* as novel regulators of BMD:

Here we highlight two DDGs that putatively impact human BMD via their roles in LMP differentiation along either an adipogenic (*Fgfrl1*) or osteogenic (*Tpx2*) trajectory, which are genes with potential roles that have been minimally characterized in the context of human BMD. Based on our previous work[7], *Fgfrl1* (fibroblast growth factor receptor-like 1) was identified as a DDG with significant human BMD GWAS associations that also colocalized with eQTL identified in the cultured fibroblast GTEx tissue (RCP = 0.1611, **Table 1**). The *Fgfrl1* network

was enriched for tradeSeq-identified genes (N = 6 genes, P_{adj} = 7.5 x 10^{-3}) for LMPs along an adipogenic trajectory (**Fig. 5A**). An increase in the expression of all tradeSeq-identified genes for the *Fgfrl1* network was observed (**Fig. 5B, Supplementary Table S12**). Importantly, the expression pattern for the tradeSeq-identified genes were consistent with the cell type boundaries established for LMPs differentiating along the adipogenic trajectory toward the MALP cell state (**Fig. 5B**). Furthermore, in the surrounding *Fgfrl1* network, two genes (*Plpp3* and *Cfap100*) have significant human BMD GWAS associations that also colocalized with sQTL in GTEx tissues, as reported in our previous study[16]. In the *Fgfrl1* network, many other genes can be associated with adipocyte function (e.g., *Lpl*, *Plpp3*, *Igfbp4*)[30–32] and the maintenance of cilia (e.g., *Cfap100*, *St5* (*Denn2b*), *Mark1*)[33–35].

The other network we identified, the *Tpx2* network, was identified for LMPs along an osteogenic trajectory (**Fig. 5C**). *Tpx2* (TPX2, microtubule-associated) is a DDG with significant human BMD GWAS associations that also colocalized with eQTL identified in the Testis GTEx tissue (RCP = 0.2031, **Table 1**). The network was enriched for tradeSeq-identified genes (N = 9 genes, P_{adj} = 5.7 x 10^{-7}) for LMPs differentiating along the osteogenic trajectory (**Fig. 5C**). Furthermore, the expression of the tradeSeq-identified genes for the *Tpx2* network were consistent with the cell type boundaries established for LMPs differentiating along the osteogenic trajectory toward the OBP (osteoblast progenitor) cell state (**Fig. 5D; Supplementary Table S10**). The expression of these genes increase as LMPs differentiate into OBPs and subsequently decrease upon reaching an OBP cell state. Additionally, *Tpx2* exhibited a significant alteration of BMD in both male and female mutant mice (Genotype P-value = 1.03 x 10^{-3}) from IMPC (**Fig. 5E**). In regards to the constituents of the *Tpx2* network, additional genes have been tested by the IMPC and result in a significant impact on BMD, such as *Ube2c*, *Top2a*,

and *Papss1*. Many other genes in the *Tpx2* network can be associated with cellular division and proliferation, including four of the genes of the kinesin family (*Kif*) motor protein genes[36]: *Kif4, Kif11, Kif15, Kif23*.

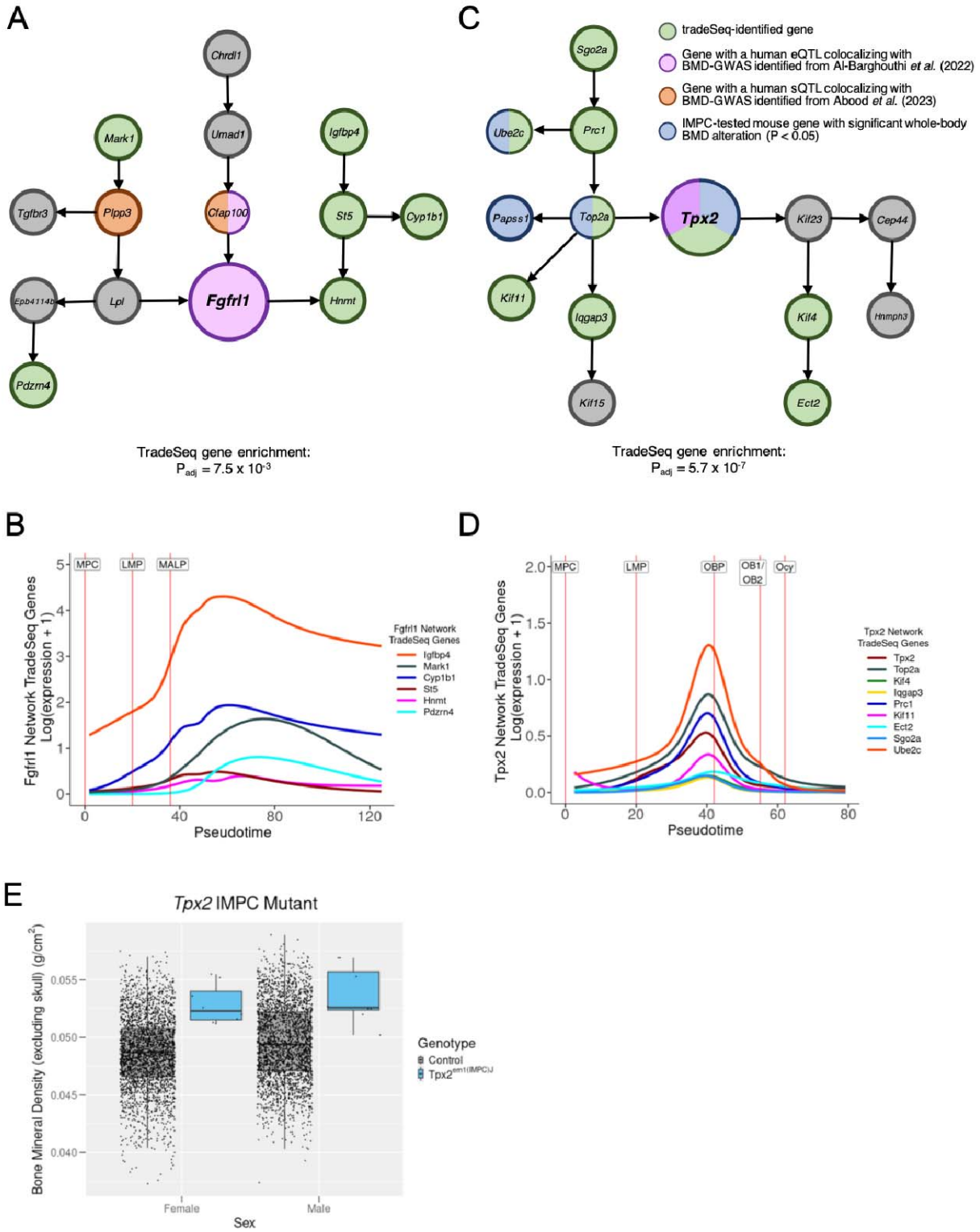

Figure 5. *Fgfrl1* and *Tpx2* are prioritized DDGs and putative drivers of mesenchymal differentiation.

Discussion

BMD GWAS has been successful at identifying thousands of SNPs associated with disease; however, the identification of causal genes and defining their functional role in disease remains challenging. The integration of "-omics" data, particularly transcriptomics, can assist in overcoming this challenge. Leveraging transcriptomics data has proven invaluable to informing GWAS, as demonstrated in studies that use these data to perform eQTL mapping, transcriptome-wide association studies (TWASs), and co-expression/gene regulatory network reconstruction. GWAS associations can colocalize with predicted sources of genetic variation that perturb causal gene function or expression, thus providing a potential mechanism through which associations impact disease. While bulk RNA-seq data has been the foundation of such analyses, scRNA-seq data can provide valuable biological context by predicting the cell type in which causal genes are affected. To inform BMD GWAS, the generation of population-scale transcriptomics data at single-cell resolution in bone-relevant cell types can assist in the discovery of novel gene targets. Here, we perform scRNA-seq on 80 DO mice to generate single-cell transcriptomics data of mesenchymal cell types relevant to bone. Using these data, our goal was to prioritize putative causal genes and provide biological context in which these genes potentially influence disease, at cell type-specific resolution. Through our pseudotemporal gene expression and network analyses, we identified 21 networks governed by predicted differentiation driver genes (DDGs) that have corresponding human BMD GWAS associations colocalizing with eQTL/sQTL in a GTEx tissue.

We demonstrate that the BMSC-OB model serves as an effective method to enrich for mesenchymal lineage cells, particularly bone-relevant cells. We characterized cells from 80 mice and identified both osteogenic and adipogenic cells derived from the mesenchymal lineage, such

as two populations of osteoblasts (OB1 and OB2), osteocyte-like cells (Ocy), and MALPs. Our trajectory inference analysis identified three distinct trajectories in which mesenchymal progenitor cells give rise to both osteogenic and adipogenic cell types, thus portraying biologically relevant and known paths of differentiation of mesenchymal progenitor cells. Pseudotemporal gene expression was analyzed along each trajectory, in a cell type-specific fashion, to identify genes that were changing the most as a function of pseudotime (tradeSeq-identified genes). Subsequent *cis*-eQTL analysis indicated that the expression of some tradeSeq-identified genes were associated with the relative proportion of cell types. While instances such as these were rare, they illustrate that the potential consequence of genetic variation impacting the expression of tradeSeq-identified genes may impact differentiation and the abundances of certain cell types along a trajectory.

To inform BMD GWAS, we utilized the scRNA-seq data in a network analysis to contextualize causal genes (and their associated networks) by predicting the cell types through which these genes are likely acting. Towards this goal, we generated cell type-specific Bayesian networks from our BMSC-OB scRNA-seq data. Our approach was similar to our previous network analyses where bulk RNA-seq data was leveraged to identify genes with strong evidence of playing central roles in networks[10,11,14]. In contrast, here we utilized scRNA-seq data to identify DDGs and prioritize networks based on the likelihood that they are involved in the differentiation of mesenchymal lineage cells (based on network connections enriched for tradeSeq-identified genes determined from inferred trajectories). Leveraging our previous work[7,16], we prioritized DDGs if they were genes with BMD GWAS associations colocalizing with human eQTL/sQTL in a GTEx tissue. Together, a gene being both a DDG and having BMD GWAS associations that colocalize with eQTL/sQTL is strong support of causality.

We identified 21 DDGs and associated networks, some of which have little to no known prior connection to bone. We contextualize these causal genes and their networks by not only providing cell type predictions in which they likely operate, but also providing information regarding the biological processes they likely affect. For example, the *Tpx2* network was identified in LMPs differentiating along an osteogenic trajectory. *Tpx2* is a microtubule assembly factor that interacts with spindle microtubules during cellular division[37]. The expression of *Tpx2* and its regulation is associated with osteosarcoma, as well as other cancers[38]. In our previous study, *Tpx2* was identified as a gene that has BMD GWAS associations that colocalize with eQTL in the Testis GTEx tissue[7]. While GTEx does not maintain bone tissue, eQTL are shared across many tissues[21]; therefore, non-bone eQTL may exert their effects in cell types associated with bone, such as LMPs, and evidence of a human eQTL effect indicates that genetic variation can modulate the expression of *Tpx2*. Additionally, when knocked out by IMPC, *Tpx2* exhibited a significant increase in whole body BMD in mice, thus providing strong support for *Tpx2* influencing the regulation of BMD in humans. In the surrounding gene neighborhood of the *Tpx2* network, other genes can be associated with cellular division as well, such as Topoisomerase 2A (*Top2a*) and the kinesin family (*Kif*) genes[36,39]. Taken together, these results indicate a potential role of *Tpx2* as a mediator of BMD and genetic variation altering its expression could affect microtubule maintenance during the expansion of osteogenic cell populations.

Additionally, the *Fgfrl1* network was identified in LMPs differentiating along an adipogenic trajectory. Fibroblast growth factor receptor-like 1 (*Fgfrl1*) is presumed to function as a decoy receptor that interacts with FGF ligands necessary for FGF signaling[40,41] and *Fgfrl1* expression is suggested to play a role in both adipogenic and osteogenic differentiation[42]. Our previous study also identified *Fgfrl1*, which has BMD GWAS associations that colocalize with

eQTL in the cultured fibroblasts GTEx tissue[14]. In the neighborhood of the *Fgfrl1* network, *Lpl*, *Plpp3*, *Igfbp4* have well-established roles in adipocyte function and metabolism[30–32]; however, other genes can be associated with cilia, such as *Cfap100*, *St5* (*Denn2b*), *Mark1*[33–35]. Interestingly, the maintenance and remodeling of cilia is essential to the differentiation of mesenchymal stem cells and pre-adipocytes (e.g., MALPs) while mature adipocytes lack cilia[43]. Moreover, the inactivation of FGF signaling is associated with the length of primary cilia[44]. Thus, genetic variation altering the expression of expression of *Fgfrl1* may affect FGF signaling to impact the maintenance of cilia and adipogenic differentiation. Additionally, given the prioritization of MALPs in the CELLECT analysis and the well-established inverse relationship between marrow adiposity and BMD[45,46], skewed balance of LMP differentiation toward marrow adipogenic cell fates may affect BMD. In summary, the *Fgfrl1* network harbors genes involved in adipogenic function, including cilia maintenance, which may contribute to LMP differentiation along an adipogenic trajectory. Together, these results indicate a potential role of *Fgfrl1* as a mediator of BMD via its role in adipogenic differentiation and maintenance of cilia.

Analyses performed here are not without limitations to consider. Our *in vitro* culturing approach and the preparation of single cells for scRNA-seq could be sources of technical variation in our study. Additionally, a pitfall of scRNA-seq is the sparsity of the resulting data, which yields an increased frequency of zero values for the expression of some genes in a proportion of cells, also known as “drop-outs”[47]. While statistical approaches can be employed to impute missing data, the accuracy of such methods and whether or not the resulting improvement in transcriptomic signal recovery is enough to warrant such intervention is contentious[48,49]. However, this issue may be partially offset given the larger scale of the scRNA-seq performed in this study and the average expression approach performed for network and eQTL analysis.

Another limitation of this study is that read alignment of the scRNA-seq data did not account for DO founder genetic variation in RNA transcripts, which could affect read mapping and gene expression measurements. An additional limitation is that the BMSC-OB model does not capture osteoclasts, another cell type associated with bone tissue. Importantly, results from our CELLECT analysis indicate that BMD heritability was not enriched for genes whose expression was more specific to osteoclast-like cells; however, these cells likely represent immature osteoclasts, as mature multinucleated cells would be too large to be captured for sequencing. Lastly, while our study employed 80 DO mice, the issue of statistical power is still a limitation; however, we demonstrate that the BMSC-OB model is amenable to high throughput and the inclusion of hundreds of mice, thus statistical power will be improved in future studies.

In summary, we showcase the use of large-scale scRNA-seq data to inform GWAS by performing a network analysis to contextualize BMD GWAS associations. Through the use of multiple single-cell analyses, we have expanded upon our understanding of the genetics of BMD. Our work exemplifies the power of single-cell transcriptomics from large populations of genetically diverse samples and our network approach for data analysis may guide future studies to consider systems genetics strategies for the discovery of genetic determinants of disease.

Methods

Sample preparation and scRNA-seq

We prepared our samples in the same fashion as performed previously in Al-Barghouthi and colleagues[15]. In brief, bone marrow was extracted from the femurs of initially 77 DO mice. BMSCs were grown to confluence after 3 days of incubation in 48-well plates and then underwent *in vitro* osteoblast differentiation for 10 days with osteogenic differentiation media (alpha MEM, 10% FBS, 1% pen/strep, 1% Glutamax, 50 μg/μL ascorbic acid [Sigma, St. Louis, MO, USA], 10 nM B-glycerophosphate [Sigma], 10 nM dexamethasome [Sigma]). After differentiation, single cells were liberated from mineralizing cultures via incubations with 60 mM ethylenediaminetetraacetic acid pH 7.4 (EDTA [Thermo Fisher Scientific], made in DPBS), 8 mg/mL collagenase (Gibco) in HBSS/4 mM CaCl2 (Fisher), and 0.25% trypsin–EDTA (Gibco). After single-cell isolation, cells from mice were pooled into groups containing cells from four to five mice total and concentrated to 800 cells/μL in PBS supplemented with 0.1% BSA (bovine serum albumin). Pooled single cells were prepared for sequencing using the 10× Chromium Controller (10× Genomics, Pleasanton, CA, USA) with the Single Cell 3' v2 reagent kit, according to the manufacturer's protocol. Libraries were sequenced on the NextSeq500 (Illumina, San Diego, CA, USA).

scRNA-seq analysis pipeline

The data was subsequently processed using the 10× Genomics Cell Ranger toolkit (version 5.0.0) using the GRCm38 reference genome[50]. Using Seurat[51] (version 4.1.0), a combined Seurat object containing all cells was generated with the inclusion of features detected in at least three cells and cells with at least 200 features detected. We used Souporcell[52] (version

2.0.0) to deconvolve the genotypes of all mice and to remove doublet cells. Cells were assigned to their associated DO mouse by making a pairwise comparison between allele calls made by the shared variants captured between Souporcell and GigaMUGA genotype arrays generated for all mice in the cohort, as previous performed in Dillard and colleagues[15]. Cell derived from two mice (176 and 244) were removed in some analyses due to poor genotyping of their respective Souporcell clusters, thus yielding a total of 75 DO mice from this study and 5 DO mice from our previous study[15] for a total of 80 DO mice. We filtered out cells with more than 6200 reads and less than 400 reads, as well as those cells with more than 10% mitochondrial reads. Further, cells were removed if they expressed greater than 20% *Rpl* and 15% *Rps* reads, which equates to cells approximately exceeding the 98 percentile. After filtering, 139,392 cells remained and the resulting object underwent standard normalization, scaling, and the top 3000 features were modeled from a variance stabilizing transformation (VST) using Seurat. Cell-cycle markers based on Tirosh and colleagues[53] were regressed out using the "CellCycleScoring" and scaling functions. For subsequent dimensionality reduction, 15 principal components (PCs) were summarized. Then, a kNN ($k = 20$) graph was created and the Louvain algorithm was used to cluster cells at a resolution of 0.5. Annotation of cell type clusters was performed manually based on differential gene expression analysis using the Seurat "FindAllMarkers" function (**Supplementary Table S1**).

For subsequent WGCNA and eQTL mapping, transcriptomic profiles for each cell type cluster were generated for each sample using a mean expression approach, as performed similarly by others[54,55]. For each sample contributing at least 5 cells to a given cluster, unnormalized unique molecular identifier (UMI) counts of gene expression for all cells in the cluster for the sample were averaged and then rounded to the nearest hundredth decimal place. A

total of 80, 80, 77, 67, 50, 76, 80 mice contributed enough cells to the MPC, LMP, OBP, OB1, OB2, Ocy, and MALP cell type clusters, respectively. Genes with non-zero expression values in fewer than 15 samples were removed. A total of 11971, 15162, 14857, 13674, 13825, 14136, and 14534 genes remained for the MPC, LMP, OBP, OB1, OB2, Ocy, and MALP clusters, respectively. Samples were normalized by computing CPMs (counts per million) without log transformation for each gene using edgeR[56] (version 4.0.7), then transformed via VST using DESeq2[57] (version 1.42.0), and quantile normalized using preprocessCore (version 1.60.2).

Trajectory and tradeSeq Analysis

Trajectory inference analysis was performed using Slingshot[58] (version 1.8.0) on the mesenchymal lineage cell clusters (seven total) of the BMSC-OB scRNA-seq data. The starting cluster was set as the MPC cluster upon the removal of a small outlier population of cells. Trajectories were inferred using 15 PCs. TradeSeq[27] (version 1.4.0) was used to analyze gene expression along the trajectories by fitting a negative binomial generalized additive model (NB-GAM) to each gene using the "fitGAM" function with nknots = 10, which was determined by using the "evaluateK" function. Prior to performing the tradeSeq analysis, the scRNA-seq data was downsampled to reduce the size of the dataset to approximately 10,000 cells (sampled at random across all seven clusters).

All cell type boundaries were established to encompass on average 78% of cells of a cell cluster (**Supplementary Table S9**). To identify genes significantly changing between boundaries in a trajectory-specific fashion, we first performed tradeSeq to compare gene expression within each trajectory (two osteogenic, one adipogenic) to highlight genes with a significant difference in expression between boundaries using the "startVsEndTest" function (**Supplementary Table S9, S10-12**). Next, we performed a global test with tradeSeq to compare

gene expression between trajectories in order to highlight genes exhibiting a significant difference in expression using the "startVsEndTest" function (**Supplementary Table S9, S13**). All tests were performed with the $\log_2$ fold change threshold (l2fc) = 0.5. For all global and trajectory-specific tests, the P-values associated with each gene were adjusted to control the false discovery rate using the "p.adjust" function from the stats (version 4.2.1) R package and genes were filtered to include those with a $P_{adj} < 0.05$.

CELLECT Analysis

CELLECT[20] (CELL-type Expression-specific integration for Complex Traits) (version 1.1.0) was used to identify likely etiologic cell types underlying complex traits of both the BMSC-OBs scRNA-seq data (**Fig. 1E, Supplementary Table S6**). CELLECT P-values were adjusted using the Bonferroni correction. CELLECT quantifies the association between the GWAS signal and cell type expression specificity using the S-LDSC genetic prioritization model[59]. Summary statistics from the UK Biobank eBMD and Fracture GWAS (Data Release 2018) and cell type annotations from each scRNA-seq data set were used as input. Cell type expression specificities were estimated using CELLEX[20] (CELL-type EXpression-specificity) (version 1.2.1) (**Supplementary Table S26**).

WGCNA

Cell type-specific mean expression matrices (as obtained above) were used as input to generate signed co-expression network modules (**Supplementary Table S7, S8**). IterativeWGCNA[22] (version 1.1.6) was used from a Singularity container built from a Docker hub image[60]. A soft threshold (power) of 14, which exceeded a R^2 threshold of 0.85 for all cell type clusters, was selected for module construction (**Supplementary Fig. 1**). Modules were

generated using iterativeWGCNA with default parameters for the "blockwiseModules" function, a minimum module size of 20 genes, minCoreKME = 0.7, and minKMEtoStay = 0.5.

Bayesian network learning

Bayesian networks were learned from each of the cell type-specific modules of co-expressed genes with the bnlearn (version 4.8.3). Gene expression matrices containing the genes for each module were used as input to the "mmhc" function which employs the Max-Min Hill Climbing algorithm (MMHC) algorithm[61] to learn the underlying structure of the Bayesian network. From the generated networks, igraph (version 1.6.0) was used to resolve 3-step neighborhoods[62]. Nodes (genes) that were unconnected to a neighborhood or connected to only one neighbor were removed. Neighborhoods were filtered to include those with a size greater than 1 standard deviation from the mean across all neighborhoods generated for the network.

DDGs (differentiation driver genes) are genes that yield large 3-step neighborhoods that are enriched ($P_{adj} < 0.05$) with tradeSeq-identified genes for a given cell type boundary. We calculated whether each neighborhood contained more tradeSeq-identified genes (for the neighborhoods' associated cell type boundary) than would be expected by chance using the hypergeometric distribution ("phyper" function) from the stats (version 4.2.1) R package. The arguments were as follows: *q*: (number of neighbors in a neighborhood that are also tradeSeq-identified genes for a given cell type boundary) – 1; *m*: total number of tradeSeq-identified genes for a given cell type boundary; *n*: (total number of identified neighborhoods) – *m*; *k*: neighborhood size (total number of neighbors); lower.tail = false. P-values were adjusted to control the false discovery rate using the "p.adjust" function from the stats (version 4.2.1) R package. These pruning steps resulted in a total of 408 DDGs and associated networks for all cell types (**Supplementary Table S16, S17-19**).

DO eQTL mapping

Prior to performing the eQTL analysis, DNA was extracted from the tails of the 80 DO mice, using the PureLink Genomic DNA mini kit (Invitrogen) and genotyped using the GigaMUGA array by Neogen Genomics (GeneSeek; Lincoln, NE). Processing and quality control of genotype data, including calculation of genotype/allele probabilities, was performed as previously described in Al-Barghouthi and colleagues[14]. Cell type-specific mean expression matrices (as obtained above) for mesenchymal lineage clusters were used as input for the eQTL mapping, which was performed using a linear mixed model (LMM) via the "scan1" function from the qtl2[63] (version 0.30) R package with allowances for the following covariates: sex, age at sacrifice (in days), weight, length, and DO mouse generation. To identify significant eQTL, we calculated a LOD (logarithm of the odds) threshold; for each cell type cluster, we chose 50 genes at random and then permuted them 1000 times using the "scan1perm" function from qtl2. We established the LOD threshold of 9.68 and 9.49 for the autosomal chromosomes and X chromosome, respectively, by taking the average of the median LOD across each cell type. A total of 563 eQTL exceeded the LOD thresholds and were no more than 1 Mbp from the transcription start site of the associated eGene (**Supplementary Table S14**).

Cell type proportion analysis

To account for technical sources of variation often retained in scRNA-seq, cell type proportions were transformed using the arcsin (asin) square root transformation from the speckle[64] R package (version 0.0.3). Tests of statistical significance were performed using the propeller t-test and ANOVA functions with default parameters. Sex of the mice and the batch each mouse was associated with for sequencing were modeled as covariates. Transformed values

were used as input for computing tests of statistical differences of cell type proportions between mice, as well as correlation to phenotypic traits (**Supplementary Table S3-S5**).

Data Availability Statement

The data that support the findings of this study are openly available in NCBI Gene Expression Omnibus database with accession codes GSE152806 and GSE269583. Processed scRNA-seq data available on Zenodo at https://zenodo.org/records/15299631.

Code Availability Statement

Code for analysis is available on GitHub at https://github.com/Farber-Lab/DO80_project.

Acknowledgements

Research reported in this publication was supported in part by the National Institute of Arthritis and Musculoskeletal and Skin Diseases of the National Institutes of Health under award numbers R01AR68345, R01AR082880, and R01AR077992 to CRF.

Author Contributions

Luke J Dillard: Writing - review & editing; Visualization; Conceptualization; Methodology; Formal analysis; Data curation; Writing - original draft. Gina M Calabrese: Methodology. Larry D Mesner: Methodology. Charles R Farber: Writing - review & editing; Funding acquisition; Supervision; Conceptualization.

Disclosures

The authors declare no competing interests.

Figure Legends

Figure 1. Analysis of single cell RNA-seq (scRNA-seq) data for BMSC-OBs derived from 80 Diversity Outbred (DO)

(A) Uniform Manifold Approximation and Projection (UMAP) of 139,392 single cells (BMSC-OBs). Cell numbers and corresponding percentages for the fifteen (15) annotated cell clusters are listed in parenthesis to the right of the annotated cluster name. **(B)** Dot plot[65] portraying representative and highly expressed genes for all annotated cell clusters. Dot color indicates the scaled gene expression while the size of the dot corresponds to the percentage of cells of a given cluster that express a given gene. **(C)** The raw proportional abundances of seven (7) mesenchymal cell clusters and one (1) cluster (Hem) representing the remain cells (i.e., mainly hematopoietic immune cells) across all 80 DO mice. **(D)** UMAP plots for mesenchymal lineage cell clusters for DO mouse 50 and DO mouse 233. **(E)** CELLECT (CELL-type Expression-specific integration for Complex Traits) cell type prioritization results displaying the Bonferroni adjusted P-values for the cell clusters. The OB1, Ocy, and MALP cell clusters (red) were significantly enriched ($P_{adj} < 0.05$, red dashed line) for BMD heritability ($P_{adj} = 0.018$, 0.010, 0.006, respectively).

Figure 2. Overview of the network analysis pipeline

Step 1: For all seven (7) of the mesenchymal lineage cell clusters (MPC, LMP, OBP, OB1, OB2, Ocy, MALP), cell type-specific co-expression modules were generated using iterative Weighted Gene Co-expression Network Analysis (iterativeWGCNA). *Step 2:* Bayesian networks were learned to generate directed networks and model causal interactions between co-expressed genes. *Step 3:* Differentiation Driver Genes (DDGs) were identified by extracting subnetworks (i.e., large 3-step neighborhood) for each gene in each cell type-specific Bayesian network and highlighting those subnetworks that were enriched ($P_{adj} < 0.05$) for trajectory-specific tradeSeq genes for the cell type boundary. *Step 4:* DDGs (and associated networks) were prioritized if the DDG was identified previously as an expression/splicing quantitative trait loci (eQTL/sQTL) that colocalized with BMD GWAS associations. Created with Biorender.com.

Figure 3. Pseudotime Trajectory Inference analysis and establishment of cell type boundaries for tradeSeq analysis

(A) Three (3) trajectories (two adipogenic, one adipogenic) were inferred from the mesenchymal cell clusters of the BMSC-OB scRNA-seq data using Slingshot. All trajectories originate from the MPC and end in either osteogenic (Ocy, OB2) or adipogenic (MALP) cell fates. **(B)** For each of the trajectories, cell type boundaries were generated using pseudotime values along the trajectories, which encompass the majority of cells of a cell type mapping to their respective trajectory. **(C)** Normalized gene expression of select genes associated with each cluster are represented in feature plots (*top*) and each gene plotted as a function of pseudotime (*bottom*) for all pseudotime trajectories (color corresponds to cell type annotation observed throughout). Vertical lines (red) represent the cell type (pseudotime) boundaries established for each cell type (label). The cell type boundary for OB1 and OB2 are represented as one red line/label for visualization purposes.

Figure 4. TradeSeq-identified genes associated with BMSC-OB differentiation exhibit eQTL effects.

(A) *Pkm* was identified as a significant global tradeSeq-identified gene (P_{adj} = 8.35 x 10^{-8}) for LMP cells along an osteogenic trajectory (LMP_to_OBP) (*left*). *S100a1* was identified as a significant global tradeSeq-identified gene (P_{adj} = 0.023) for OBP cells along osteogenic trajectory 1 (OBP_to_OB1) (*right*). **(B)** Plots indicating the cell type-specific expression quantitative trait loci (eQTL) signal for both *Pkm* and *S100a1*. A negative eQTL effect on *Pkm* expression was observed in LMPs for Diversity Outbred (DO) mice with a PWK haplotype background at the *Pkm* locus (*left*). A positive eQTL effect on the expression of *S100a1* was observed in OBPs for DO mice with a 129 haplotype background at the *S100a1* locus, while a negative effect was observed for NZO mice (*right*). **(C)** The expression of *Pkm* and *S100a1* based on DO mouse (expression values transformed via variance stabilizing transformation (VST), as described in Methods). Genotype abbreviations correspond to DO haplotype background (legend) at the respective gene locus. Mice with at least one PWK allele (genotype abbreviation G) tend to have decreased expression of *Pkm* (*left*). Mice with at least one 129 allele (genotype abbreviation C) tend to have increased expression of *S100a1*, while NZO mice (genotype abbreviation E) have decreased expression (*right*). **(D)** PWK mice had a significant reduction in mature osteoblasts (OB1) and osteocyte-like cells (Ocy) proportions relative to other mice (P = 0.030 and P = 0.026, respectively; t-test), while LMP proportions were unaffected. Asterisks represent any of the other haplotype backgrounds. 129 mice showed a significant decrease in LMP proportion and increase in OB1 proportion (P = 0.008 and P = 0.016, respectively; t-test), but OBP proportions were unaffected. No significant effects on cell type proportions were observed in NZO mice (**Supplementary Fig. 2**).

Figure 5. *Fgfrl1* and *Tpx2* are prioritized DDGs and putative drivers of mesenchymal differentiation.

(A) *Fgfrl1* was identified as a Differentiation Driver Gene (DDG) of a network for LMPs differentiating along an adipogenic trajectory. The network is enriched (P_{adj} = 7.5 x 10^{-3}) for trajectory-specific tradeSeq-identified genes for the LMP_to_MALP cell type boundary (*Hnmt, St5, Igfbp4, Cyp1b1, Pdzrn4, Mark1*). *Fgfrl1* was previous identified as a gene that has BMD GWAS associations that colocalize with an eQTL in the cultured fibroblast GTEx tissue. **(B)** An increase in the expression of tradeSeq-identified genes coincides with the LMP_to_MALP cell type boundary in which they were identified as significant. **(C)** *Tpx2* was identified as a DDG of a network for LMPs differentiating along an osteogenic trajectory. The network is enriched (P_{adj} = 5.7 x 10^{-7}) for tradeSeq-identified genes for the LMP_to_OBP cell type boundary (*Tpx2, Top2a, Kif4, Iqgap3, Prc1, Kif11, Ect2, Sgo2a, Ube2c*). *Tpx2* is both a tradeSeq gene and previously identified as a gene that has BMD GWAS associations that colocalize with an eQTL in the Testis GTEx tissue. **(D)** An increase in the expression of tradeSeq-identified genes coincides with the LMP_to_OBP cell type boundary in which they were identified as significant. **(E)** Box plot displaying whole-body bone mineral density (BMD) measurements (excluding skull) from the International Mouse Knockout Consortium (IMPC) for *Tpx2* mutant mice, which exhibited a significant increase in BMD (Genotype P-value = 1.03 x 10^{-3}) in both male and female mice (N = 8 (M) and 8 (F) mutants; N = 2574 (M) and 2633 (F) controls)

References

1. Lin, J. T. & Lane, J. M. Osteoporosis: a review. *Clin. Orthop. Relat. Res.* 126–134 (2004).
2. Peacock, M., Turner, C. H., Econs, M. J. & Foroud, T. Genetics of osteoporosis. *Endocr. Rev.* **23**, 303–326 (2002).
3. Johnell, O. *et al.* Predictive value of BMD for hip and other fractures. *J. Bone Miner. Res.* **20**, 1185–1194 (2005).
4. Morris, J. A. *et al.* An atlas of genetic influences on osteoporosis in humans and mice. *Nat. Genet.* **51**, 258–266 (2019).
5. Cookson, W., Liang, L., Abecasis, G., Moffatt, M. & Lathrop, M. Mapping complex disease traits with global gene expression. *Nat. Rev. Genet.* **10**, 184–194 (2009).
6. Wen, X., Pique-Regi, R. & Luca, F. Integrating molecular QTL data into genome-wide genetic association analysis: Probabilistic assessment of enrichment and colocalization. *PLoS Genet.* **13**, e1006646 (2017).
7. Al-Barghouthi, B. M. *et al.* Transcriptome-wide association study and eQTL colocalization identify potentially causal genes responsible for human bone mineral density GWAS associations. *Elife* **11**, (2022).
8. Li, B. & Ritchie, M. D. From GWAS to Gene: Transcriptome-Wide Association Studies and Other Methods to Functionally Understand GWAS Discoveries. *Front. Genet.* **12**, 713230 (2021).
9. Akiyama, M. Multi-omics study for interpretation of genome-wide association study. *J. Hum. Genet.* **66**, 3–10 (2020).
10. Calabrese, G. M. *et al.* Integrating GWAS and Co-expression Network Data Identifies Bone Mineral Density Genes SPTBN1 and MARK3 and an Osteoblast Functional Module. *Cell Syst* **4**, 46-59.e4 (2017).
11. Sabik, O. L., Calabrese, G. M., Taleghani, E., Ackert-Bicknell, C. L. & Farber, C. R. Identification of a Core Module for Bone Mineral Density through the Integration of a Co-expression Network and GWAS Data. *Cell Rep.* **32**, 108145 (2020).
12. GTEx Consortium. The Genotype-Tissue Expression (GTEx) project. *Nat. Genet.* **45**, 580–585 (2013).
13. GTEx Consortium. The GTEx Consortium atlas of genetic regulatory effects across human tissues. *Science* **369**, 1318–1330 (2020).
14. Al-Barghouthi, B. M. *et al.* Systems genetics in diversity outbred mice inform BMD GWAS and identify determinants of bone strength. *Nat. Commun.* **12**, 3408 (2021).
15. Dillard, L. J. *et al.* Single-Cell Transcriptomics of Bone Marrow Stromal Cells in Diversity Outbred Mice: A Model for Population-Level scRNA-Seq Studies. *J. Bone Miner. Res.* **38**, 1350–1363 (2023).
16. Abood, A. *et al.* Long-read proteogenomics to connect disease-associated sQTLs to the protein isoform effectors of disease. *bioRxiv* 2023.03.17.531557 (2023) doi:10.1101/2023.03.17.531557.
17. Bogue, M. A., Churchill, G. A. & Chesler, E. J. Collaborative Cross and Diversity Outbred data resources in the Mouse Phenome Database. *Mamm. Genome* **26**, 511–520 (2015).
18. Churchill, G. A., Gatti, D. M., Munger, S. C. & Svenson, K. L. The Diversity Outbred mouse population. *Mamm. Genome* **23**, 713–718 (2012).
19. Zhong, L. *et al.* Single cell transcriptomics identifies a unique adipose lineage cell population that regulates bone marrow environment. *Elife* **9**, (2020).

20. Timshel, P. N., Thompson, J. J. & Pers, T. H. Genetic mapping of etiologic brain cell types for obesity. *Elife* **9**, (2020).
21. GTEx Consortium *et al.* Genetic effects on gene expression across human tissues. *Nature* **550**, 204–213 (2017).
22. Greenfest-Allen, E., Cartailler, J.-P., Magnuson, M. A. & Stoeckert, C. J. iterativeWGCNA: iterative refinement to improve module detection from WGCNA co-expression networks. *bioRxiv* 234062 (2017) doi:10.1101/234062.
23. Chan, C. K. F. *et al.* Identification of the Human Skeletal Stem Cell. *Cell* **175**, 43-56.e21 (2018).
24. Mizuhashi, K. *et al.* Resting zone of the growth plate houses a unique class of skeletal stem cells. *Nature* **563**, 254–258 (2018).
25. Debnath, S. *et al*. Discovery of a periosteal stem cell mediating intramembranous bone formation. *Nature* **562**, 133–139 (2018).
26. Matsushita, Y. *et al.* A Wnt-mediated transformation of the bone marrow stromal cell identity orchestrates skeletal regeneration. *Nat. Commun.* **11**, 332 (2020).
27. Van den Berge, K. *et al.* Trajectory-based differential expression analysis for single-cell sequencing data. *Nat. Commun.* **11**, 1201 (2020).
28. Thomas, P. D. *et al.* PANTHER: Making genome-scale phylogenetics accessible to all. *Protein Sci.* **31**, 8–22 (2022).
29. Groza, T. *et al.* The International Mouse Phenotyping Consortium: comprehensive knockout phenotyping underpinning the study of human disease. *Nucleic Acids Res.* **51**, D1038–D1045 (2023).
30. Enerbäck, S., Ohlsson, B. G., Samuelsson, L. & Bjursell, G. Characterization of the human lipoprotein lipase (LPL) promoter: evidence of two cis-regulatory regions, LP-alpha and LP-beta, of importance for the differentiation-linked induction of the LPL gene during adipogenesis. *Mol. Cell. Biol.* **12**, 4622–4633 (1992).
31. Federico, L. *et al.* Lipid phosphate phosphatase 3 regulates adipocyte sphingolipid synthesis, but not developmental adipogenesis or diet-induced obesity in mice. *PLoS One* **13**, e0198063 (2018).
32. Maridas, D. E., DeMambro, V. E., Le, P. T., Mohan, S. & Rosen, C. J. IGFBP4 Is Required for Adipogenesis and Influences the Distribution of Adipose Depots. *Endocrinology* **158**, 3488–3500 (2017).
33. Sigg, M. A. *et al.* Evolutionary Proteomics Uncovers Ancient Associations of Cilia with Signaling Pathways. *Dev. Cell* **43**, 744-762.e11 (2017).
34. Kumar, R. *et al.* A cell-based GEF assay reveals new substrates for DENN domains and a role for DENND2B in primary ciliogenesis. *Sci Adv* **8**, eabk3088 (2022).
35. Fumoto, K. *et al.* Mark1 regulates distal airspace expansion through type I pneumocyte flattening in lung development. *J. Cell Sci.* **132**, (2019).
36. Miki, H., Setou, M., Kaneshiro, K. & Hirokawa, N. All kinesin superfamily protein, KIF, genes in mouse and human. *Proc. Natl. Acad. Sci. U. S. A.* **98**, 7004–7011 (2001).
37. Zhang, R., Roostalu, J., Surrey, T. & Nogales, E. Structural insight into TPX2-stimulated microtubule assembly. *Elife* **6**, (2017).
38. Zhu, D., Xu, X., Zhang, M. & Wang, T. TPX2 regulated by miR-29c-3p induces cell proliferation in osteosarcoma via the AKT signaling pathway. *Oncol. Lett.* **23**, 143 (2022).
39. Uusküla-Reimand, L. & Wilson, M. D. Untangling the roles of TOP2A and TOP2B in transcription and cancer. *Sci Adv* **8**, eadd4920 (2022).

40. Trueb, B. Biology of FGFRL1, the fifth fibroblast growth factor receptor. *Cell. Mol. Life Sci.* **68**, 951–964 (2011).
41. Steinberg, F. *et al.* The FGFRL1 receptor is shed from cell membranes, binds fibroblast growth factors (FGFs), and antagonizes FGF signaling in Xenopus embryos. *J. Biol. Chem.* **285**, 2193–2202 (2010).
42. Kähkönen, T. E. *et al.* Role of fibroblast growth factor receptors (FGFR) and FGFR like-1 (FGFRL1) in mesenchymal stromal cell differentiation to osteoblasts and adipocytes. *Mol. Cell. Endocrinol.* **461**, 194–204 (2018).
43. Hilgendorf, K. I. Primary Cilia Are Critical Regulators of White Adipose Tissue Expansion. *Front. Physiol.* **12**, 769367 (2021).
44. Neugebauer, J. M., Amack, J. D., Peterson, A. G., Bisgrove, B. W. & Yost, H. J. FGF signalling during embryo development regulates cilia length in diverse epithelia. *Nature* **458**, 651–654 (2009).
45. Fazeli, P. K. *et al.* Marrow fat and bone--new perspectives. *J. Clin. Endocrinol. Metab.* **98**, 935–945 (2013).
46. Veldhuis-Vlug, A. G. & Rosen, C. J. Clinical implications of bone marrow adiposity. *J. Intern. Med.* **283**, 121–139 (2018).
47. Haque, A., Engel, J., Teichmann, S. A. & Lönnberg, T. A practical guide to single-cell RNA-sequencing for biomedical research and clinical applications. *Genome Med.* **9**, 75 (2017).
48. Cheng, Y., Ma, X., Yuan, L., Sun, Z. & Wang, P. Evaluating imputation methods for single-cell RNA-seq data. *BMC Bioinformatics* **24**, 302 (2023).
49. Yu, X., Abbas-Aghababazadeh, F., Chen, Y. A. & Fridley, B. L. Statistical and Bioinformatics Analysis of Data from Bulk and Single-Cell RNA Sequencing Experiments. *Methods Mol. Biol.* **2194**, 143–175 (2021).
50. Church, D. M. *et al.* Lineage-specific biology revealed by a finished genome assembly of the mouse. *PLoS Biol.* **7**, e1000112 (2009).
51. Hao, Y. *et al.* Integrated analysis of multimodal single-cell data. *Cell* **184**, 3573-3587.e29 (2021).
52. Heaton, H. *et al.* Souporcell: robust clustering of single-cell RNA-seq data by genotype without reference genotypes. *Nat. Methods* **17**, 615–620 (2020).
53. Tirosh, I. *et al.* Dissecting the multicellular ecosystem of metastatic melanoma by single-cell RNA-seq. *Science* **352**, 189–196 (2016).
54. Neavin, D. *et al.* Single cell eQTL analysis identifies cell type-specific genetic control of gene expression in fibroblasts and reprogrammed induced pluripotent stem cells. *Genome Biol.* **22**, 76 (2021).
55. van der Wijst, M. G. P. *et al.* Single-cell RNA sequencing identifies celltype-specific cis-eQTLs and co-expression QTLs. *Nat. Genet.* **50**, 493–497 (2018).
56. Robinson, M. D., McCarthy, D. J. & Smyth, G. K. edgeR: a Bioconductor package for differential expression analysis of digital gene expression data. *Bioinformatics* **26**, 139–140 (2010).
57. Love, M. I., Huber, W. & Anders, S. Moderated estimation of fold change and dispersion for RNA-seq data with DESeq2. *Genome Biol.* **15**, 550 (2014).
58. Street, K. *et al.* Slingshot: cell lineage and pseudotime inference for single-cell transcriptomics. *BMC Genomics* **19**, 477 (2018).

59. Finucane, H. K. *et al.* Partitioning heritability by functional annotation using genome-wide association summary statistics. *Nat. Genet.* **47**, 1228–1235 (2015).
60. Cartailler, J. P. *Iterativewgcna*. (2022).
61. Tsamardinos, I., Brown, L. E. & Aliferis, C. F. The max-min hill-climbing Bayesian network structure learning algorithm. *Mach. Learn.* **65**, 31–78 (2006).
62. Porter, M. D. & Smith, R. Network neighborhood analysis. in *2010 IEEE International Conference on Intelligence and Security Informatics* (IEEE, 2010). doi:10.1109/isi.2010.5484781.
63. Broman, K. W. *et al.* R/qtl2: Software for Mapping Quantitative Trait Loci with High-Dimensional Data and Multiparent Populations. *Genetics* **211**, 495–502 (2019).
64. Phipson, B. *et al.* propeller: testing for differences in cell type proportions in single cell data. *Bioinformatics* **38**, 4720–4726 (2022).
65. Marsh, S., Salmon, M. & Hoffman, P. *Custom Visualizations & Functions for Streamlined Analyses of Single Cell Sequencing*. (2023). doi:10.5281/zenodo.7534950.